ACS APPLIED MATERIALS & INTERFACES

Research Article

Cite This: ACS Appl. Mater. Interfaces 2018, 10, 41070−41075

www.acsami.org

Epidermis-Inspired Ultrathin 3D Cellular Sensor Array for Self-Powered Biomedical Monitoring

Cheng Yan,[†] Weili Deng,*[,†] Long Jin,[†] Tao Yang,[†] Zixing Wang,[†] Xiang Chu,[†] Hai Su,[†] Jun Chen,*[,§] and Weiqing Yang*[,†,‡]

[†]Key Laboratory of Advanced Technologies of Materials (Ministry of Education), School of Materials Science and Engineering, and [‡]State Key Laboratory of Traction Power, Southwest Jiaotong University, Chengdu 610031, China

[§]Department of Materials Science and Engineering, Stanford University, Stanford, California 94305, United States

Supporting Information

ABSTRACT: Sensing devices with wearability would open the door to many advanced applications including soft robotics, artificial intelligence, and healthcare monitoring. Here, inspired by the configuration of the human epidermis, we present a flexible three-dimensional (3D) cellular sensor array (CSA) via a one-step thermally induced phase separation method. The CSA was framed by the 3D cellular electret with caged piezoelectric nanoparticles, which was ultrathin (80 μm), lightweight, and highly robust. For biomedical sensing, the 3D-CSA holds a decent pressure sensitivity up to 0.19 V kPa^{-1} with a response time of less than 16 ms. Owing to its rigid structural symmetry, the 3D-CSA could be identically operated from its both sides. It was demonstrated to successfully measure the human heartbeat, detect the eyeball motion for sleeping monitoring, and tactile imaging. Mimicking the functionalities of the human skin with a self-powered operation feature, the 3D-CSA was expected to represent a substantial advancement in wearable electronics for healthcare.

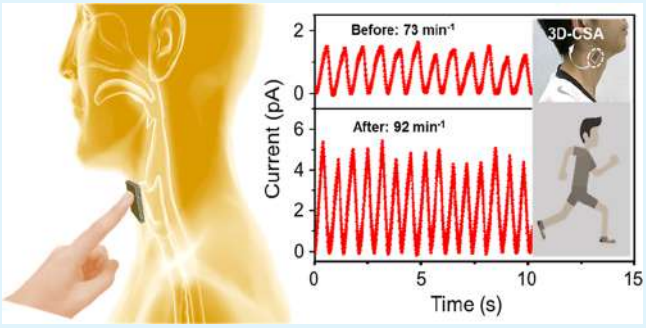

KEYWORDS: *epidermis, ultrathin, cellular sensor array, self-powered, biomedical monitoring*

INTRODUCTION

With great potential of revolutionizing our way of living, rapidly increasing research progress has been made in the field of wearable electronics for healthcare monitoring.[1−16] One critical challenge identified in this field is how to power up the functioning devices in the lightweight, flexible/stretchable electronics system.[17−19] To overcome the challenge, on one hand, a flexible thin battery provides a potential solution.[20−22] However, the flexibility and thinness requirement of the battery largely compromise its electrochemical performance.[23] Besides, made from toxic chemicals, safety is also another serious concern for the wearable battery.[24−26] On the other hand, human body naturally contains plenty of biomechanical energy. A sustainable power source could be realized if technology could convert the human biomechanical motions into electricity.[27−29] Flexible nanogenerators and self-powered electronics emerge to alternatively pave such a creative way to solve the puzzle for the wearable electronics.[30−40] However, most current reports are not sufficiently thin and flexible to accommodate to the human skin curvature. As a porous thin-film material, cellular polypropylene (PP) electret with favorable flexibility could directly generate electrical signals in response to mechanical force by means of piezoelectric effect, which offers an alternative strategy for either wearable power generation or sensing.[41−44] Bioinspired structral design in sensing devices is desired but underexplored to realize a harmonisous connnetion with human skin.[45] In addition, most of the reported wearable sensors can only effectivley operate from one side of the device, which also places a challenge for the demand of seamless, bidirectional interfaces for sensing.[46]

Herein, inspired by the human epidermis, we present an ultrathin three-dimensional cellular sensor array (3D-CSA) with a rigid structure/function symmetry via scalable fabrication techniques for self-powered biomedical monitoring. Constructed by the 3D cellular electret with caged piezoelectric nanoparticles via a one-step thermally induced phase separation (TIPS) method, the 3D-CSA was as thin as 80 μm, and well conformable with the curved skin surface for measurement. With a decent pressure sensitivity of 0.19 V kPa^{-1} and a response time of less than 16 ms, the 3D-CSA was demonstrated to perform human heartbeat measurement and eyeball motion monitoring during sleeping, with identical sensing performance from both sides. Given the combinatorial advantages of low-cost, thinness, flexibility, structural symme-

Received: August 22, 2018
Accepted: November 6, 2018
Published: November 6, 2018

DOI: 10.1021/acsami.8b14514
ACS Appl. Mater. Interfaces 2018, 10, 41070−41075

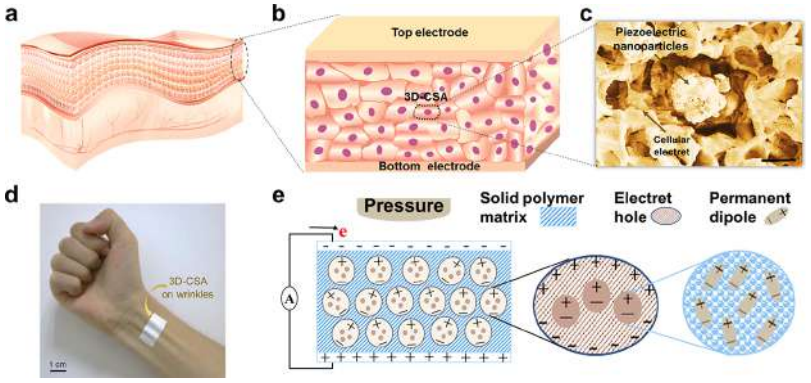

Figure 1. Structure design and working principle of the epidermis-inspired 3D-CSA. (a) Schematic illustration showing the structure of the human epidermis. (b) Sketch of the 3D-CSA, mimicking the structure of the human epidermis. (c) SEM image showing the structure of a cellular sensor unit, which is composed of the electret matrix and piezoelectric nanoparticles (scale bar: 2 μm). (d) Photograph of the ultrathin flexible 3D-CSA with a thickness of 80 μm. (e) Illustration showing the working principle of the 3D-CSA.

try, and scalability in the material synthesis and device fabrication, the 3D-CSA is unique and represents a solid advancement in the field of skin electronics for biomedical applications.

EXPERIMENTAL SECTION

Preparing Cellular PP/PZT Composite Framework. Three components, PP (30% weight ratio), mixed diluent [the weight ratio of dibutyl phthalate (DBP) and soybean oil was 3:2], and lead zirconate titanate (PZT) nanoparticles, were mixed in a three-necked flask with one inlet for argon, another for the condenser, and a third for the test thermocouple. The flask was placed on the hot plate at a temperature of 463 K with a magnetic stirring speed of 500 rpm for 30 min. Then, the mixture was cooled down to room temperature (RT) to yield a homogeneous solution. Next, the solidified mixture was cut into small pieces and sandwiched by two slides of cover slips, which was placed onto a hot plate at 463 K. The remained diluent in the membrane was extracted by *n*-hexane for 24 h at RT and dried in a vacuum oven at 313 K for 12 h to finally obtain the cellular PP/PZT composite framework.

Polarization of the Films. The film was placed on the hot plate at 323 K. The corona discharge was applied to one side of the sample with a voltage of −18 kV for 60 s. The vertical distance between the needle tip and the film was 4 cm. Another side of the electrode was connected to ground while charging. Both electrodes were shorted after the discharge treatment.

Characterization of 3D-CSA. The morphologies of the samples were characterized by a field-emission scanning electron microscopy (SEM, JSM-7001F). The applied external force was measured by a force sensor (RF-Cx-ST). The output voltage signals of the sensor were measured by a low-noise voltage preamplifier (Keithley-6514 system electrometer). The output current signals of the sensor were measured by a low-noise current preamplifier (Stanford Research SR570).

RESULTS AND DISCUSSION

Mimicked from the tridimensional epidermis of the human skin, the 3D-CSA holds a sandwich structure consisting of one functional layer and two electrode layers, as the illustration shown in Figure 1. In order to obtain the features of lightweight, thinness, biocompatibility, and low-cost, PP was selected to construct a 3D cellular framework via the TIPS method (Figure S1), and the piezoelectric PZT nanoparticles were embedded and distributed at the cellular centers as the functional layer. Two layers of copper with a thickness of 130 nm were respectively deposited onto both sides of the functional layer as electrodes and protection layers, as schematically shown in Figure 1a,b. A cross-section view of the CSA via SEM is displayed in Figure 1c, which indicates that the 3D cellular PP electret with embedded PZT nanoparticles were structurally alike to the stratum spinosum. Employing the ultrathin medical double tape as a uniform adhesive layer to enhance the stability upon bending and forming, the as-fabricated 3D-CSA device with a thickness of 80 μm is shown in Figure 1d, exhibited excellent conformability that well accommodated to the skin curvature. As discussed in the Experimental Section, the fabrication process of the 3D-CSA is straightforward and compatible with possible large-scale manufacturing. The working principle of the 3D-CSA was elucidated in Figure 1e. To measure the applied pressure with electrical signals, a first step was to polarize the thin film under a high voltage of −18 kV, with a result that the air in the gap of the cellular film was ionized and dissociated. The polarization serves two purposes. First, it will engender charges with opposite polarity on both sides of air bubbles. Second, it will initiate the dipole orientation in the PZT nanoparticles. Theoretically, the 3D-CSA can be simplified as a multilayered structure with vertically aligned PP−piezoelectric nanoparticle-filled air (PNPFA)−PP, the charge density on the copper electrode σ_0 can be expressed as (see the Supporting Information Note 1 for detailed derivation)

$$\sigma_0 = \frac{\varepsilon \frac{1}{n} \sum_{i=1}^{n} \sigma_i}{\varepsilon + D_1/D_2} \quad (1)$$

where ε is the relative dielectric constant of PP, n is the layer number of PNPFA in vertical direction, and each layer of PNPFA carries a total planner charge density of σ_i and $-\sigma_i$. D_2 and D_1, respectively, represent the total thickness of PNPFA and PP between the bottom and top electrode. From eq 1, it can be seen that the total charge density σ_0 is directly proportional to the amount of the charge density of each layer, inversely proportional to the ratio of the thicknesses of PP and PNPFA. Then, if the value of D_1/D_2 is changed under external force, the device will have a potential difference between the opposite electrodes. Once the external pressure was applied, device deformation mainly comes from the inside air gap because the Young's modulus of solid media is several orders of magnitude higher than that of air. Namely, the thickness of PNPFA D_2 will decrease, whereas D_1 stays nearly constant. The reduction of D_2 will bring deformation into the embedded piezoelectric nanoparticles, resulting in a reduction of charge

DOI: 10.1021/acsami.8b14514
ACS Appl. Mater. Interfaces 2018, 10, 41070−41075

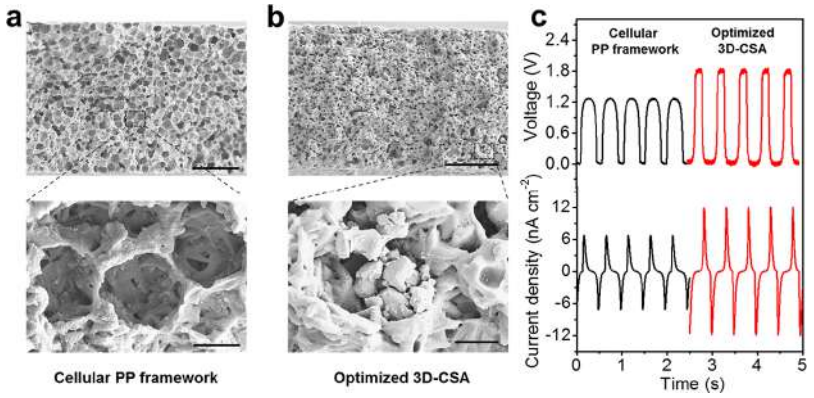

Figure 2. Device structure optimization. (a) SEM image showing the cross-sectional view of the cellular PP framework with 60% weight ratio of DBP (scale bar: 25 μm) and the enlarged view of a cellular structure (scale bar: 2.5 μm). (b) SEM image showing the cross-sectional view of the cellular PP framework with 30% weight ratio of PZT nanoparticles (scale bar: 25 μm) and an enlarged view of a cellular construction (scale bar: 2.5 μm). (c) Comparison of the voltage and current density of the CSA, the pressure applied on the sensor was 6.4 kPa. Black lines represent the electric output of the cellular PP framework, whereas red lines represent the output of the optimized 3D-CSA.

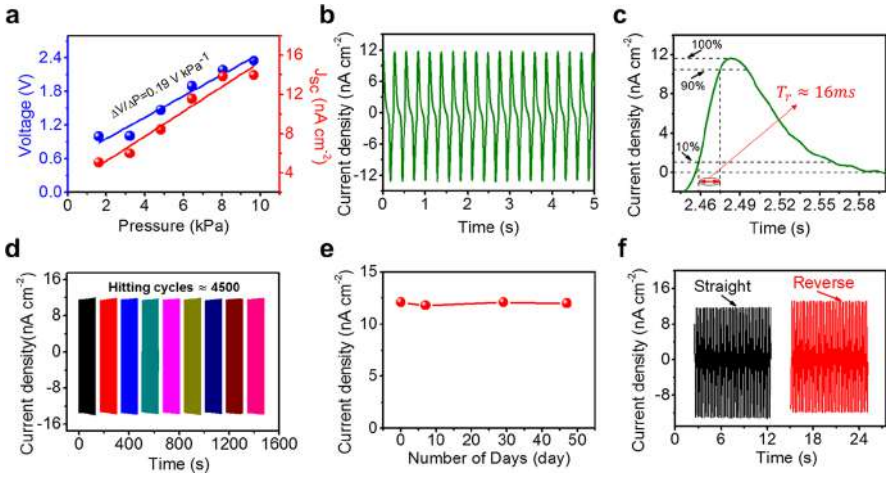

Figure 3. Electrical and mechanical characterization of the 3D-CSA. (a) Measurement of the device sensitivity via current and voltage signals under varying applied forces. (b) Short-circuit current density of the 3D-CSA upon a constant pressure. (c) Measurement of the response time of the 3D-CSA. T_r represents the rise time. (d) Mechanical durability test. (e) Electric output of the device is very air-stable for more than 45 days in ambient environment. (f) 3D-CSA can be operated from either side with identical electrical output.

density on the bottom and top electrodes. As indicated in Figure S2 and Video S1 (Supporting Information), at the original stage I, without device deformation, the electric potential between the top and bottom electrode of the 3D-CSA is zero. When the device was compressed, the current flows from the bottom electrode to the upper electrode, as demonstrated in stage II. With further device deformation, the charge density on the electrode of the 3D-CSA will decrease until a new equilibration is established. Meanwhile, the electrical potential difference between the bottom and top electrode reaches the maximum value, as illustrated in stage III. When the applied pressure withdrew, the 3D-CSA will return to its original state owing to the elasticity of the PP framework, the charge density on both electrodes of the 3D-CSA will ascend, resulting in current flowing from the upper electrode to the bottom electrode, as demonstrated in stage IV. As a consequence, structurally mimicking from the human tridimensional epidermis, the 3D-CSA could convert the touch force into an electrical signal for biomedical sensing.

To create an electret-caged structure with filled piezoelectric nanoparticles like a cell structure in the epidermis, a one-step TIPS method (details in the Experimental Section) was used for material synthesis and structure optimization, as exhibited in Figure S3. The corresponding SEM image of the cellular PP framework with 60% weight ratio of DBP is shown in Figure 2a. The 60% weight ratio was an optimized setting parameter. A higher weight ratio of DBP will bring an enhancement of the piezoelectric charges for better electrical output; however, the higher DBP amount will also destruct the cellular structure and result in current leakage. A detailed analysis of the impact of the DBP amount on the device performance was elaborated in the Supporting Information Note 2. An enlarged view of the cellular structure indicates a hollow cell morphology. To further enhance the performance , PZT nanoparticles with an average size of 0.74 μm (Figure S4) were employed as the caged piezoelectric nanoparticles to fill in the hollow of the cells. As shown in Figure 2b, with the increase of the PZT doping ratio, the intensity of peaks corresponding to PZT in the composite film increases, indicating the ascent of perovskite phases (Figure S5). In addition, the caged composite with 30% weight ratio of PZT nanoparticles exhibited the maximal electric output performance (Supporting Information Note 3). To affirm the optimized validity of the electret-caged structure, a comparison of the voltage and

DOI: 10.1021/acsami.8b14514
ACS Appl. Mater. Interfaces 2018, 10, 41070−41075

current density of the CSA was presented at a pressure of 6.4 kPa (Figure 2c), which indicates that voltage and current density with structure optimization are, respectively, increased by about 1.5 and 1.8 times than that of pure cellular PP. The enhancement was mainly attributed to the synergistic piezoelectric effects between the aligned dipoles in PZT nanoparticles and ionization decomposition of the air in the cellular PP framework.

In order to further characterize the performance of the as-fabricated 3D-CSA, a series of tests were carried out. As shown in Figure 3a, the 3D-CSA was tested under varying applied forces, indicating an excellent sensitivity of 0.19 V kPa^{-1} compared with the reported results of its kind (Table S1). At a constant pressure of 6.4 kPa, 3D-CSA attained an current density of 11.9 nA cm^{-2}, as demonstrated in Figure 3b. The response time is another important parameter of the 3D-CSA as a sensor, which was defined as the time period of current density changing from 10 to 90% of its peak value. The rise time T_r was shown in Figure 3c, indicating a response time of less than 16 ms, which could assure the quick response of the device to the external pressure for self-powered biomedical sensing. In addition, to further investigate the mechanical durability, the 3D-CSA was operated with a repetitive extrusion force of 6.4 kPa for more than 4500 cycles, as exhibited in Figure 3d. The current density amplitudes show negligible changes during the test, which indicates a good durability of the 3D-CSA. Besides, packaged with a medical tape, oxidization of the electrode was well avoided, and the electrical output of the 3D-CSA was kept constant after 47 days in the ambient environment, as shown in Figures 3e and S6, demonstrating the high charge storage stability of the device. Owing to its structure symmetry, the 3D-CSA can be operated from either side with identical electrical output, as shown in Figure 3f, which would unlock new strategies of developing seamless, bidirectional interfaces between humans and machines for advanced applications.

Owing to the compelling features of lightweight, thinness, flexibility, and biocompatibility, the 3D-CSA can be easily attached to the human skin of various body parts for self-powered biomedical sensing, as the sketch exhibited in Figure 4a. Moreover, the 3D-CSA was composed of plentiful mircroscale cellular sensor units, blood pressure induced vessel expansion could be well delivered and perceived by many of the sensor units for reliable and accurate sensing. To demonstrate its capability, three sets of practical applications were demonstrated. First, the 3D-CSA was tightly attached to the human carotid artery with ultrathin medical double tape to measure the human heartbeat during physical exercise for healthcare monitoring, as shown in Figure 4b. The tester exhibited a heartbeat rate of 73 times per minute at rest and 92 times per minute after running (Video S2). And the larger pulse amplitudes and higher frequencies were clearly indicated in the heart rate waveform after 30 min running. Second, as exhibited in Figure 4c and Video S3, the 3D-CSA is so soft and conformable that it can detect the eyeball motion when attached to the human canthus. During one slight wink, the generated electrical singnal comprises of three main parts, labeled as preparatory stage (A), eye-closed stage (B), and goggle stage (C). It is highly subjected to the eyeball motion state, which could be used either for sleeping disorder diagnosis or triggering signals to warn the driver with fatigue.

In addition, the 3D-CSA can also be applied for self-powered tactile imaging. As shown in Figure 4d and Video S4,

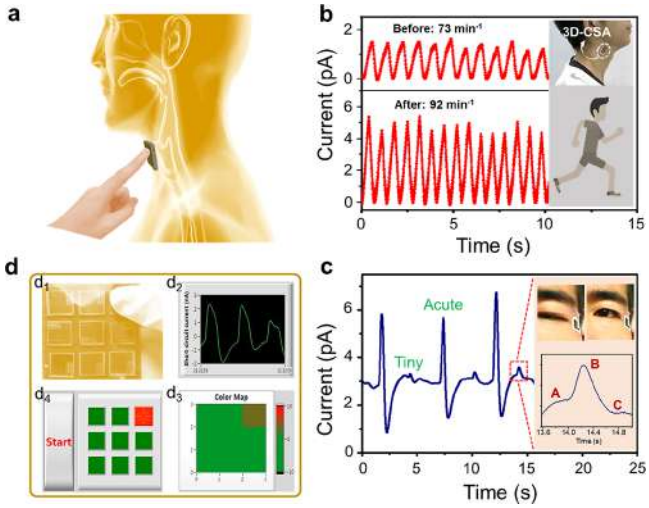

Figure 4. Demonstration of the 3D-CSA array for wearable biomedical monitoring. (a) Schematic illustration showing that the 3D-CSA can be easily attached to the human skin for biomechanical monitoring. (b) 3D-CSA measures the human heartbeat. (c) 3D-CSA is so soft and conformable that it can even detect the eyeball motion. (d) 3D-CSA can also be applied for self-powered tactile imaging and monitoring the local gentle touching of human fingers.

3 by 3 units of the 3D-CSA were fabricated to monitor the local touching action of fingers. The generated electrical signals were acquired and displayed via LabVIEW programming. When a random unit was touched (Figure 4d_1), current signals were generated, as shown in Figure 4d_2. To scale up, nine different positions on the array were pressed by a square plate (area: 0.8 × 0.8 cm^2), and the current remained stable with negligible fluctuation (Figure S7). Moreover, the generated electric signals of the 3D-CSA could be used to express the applied pressure via visualizing it in the forms of color change (Figure 4d_3) and on/off switch (Figure 4d_4) of a square LED in the Labview.

CONCLUSIONS

In summary, inspired by the human epidermis, an ultrathin, biocompatible, and highly sensitive wearable sensor was developed based on the 3D cellular electret with caged piezoelectric nanoparticles for self-powered biomedical monitering. Via a one-step TIPS method, the 3D-CSA could be massively produced. Owing to the rigid symmetric structure, the 3D-CSA was demonstrated to measure the human heartbeat, monitor eyeball motions, and perform active tactile imaging . The 3D-CSA represents a solid advancement in the field of skin electronics, which may unlock new applications in the fields of healthcare monitoring, artificial intelligence, and human computer interface.

ASSOCIATED CONTENT

Supporting Information

The Supporting Information is available free of charge on the ACS Publications website at DOI: 10.1021/acsami.8b14514.

Fabrication process of the 3D-CSA; working mechanism of the 3D-CSA in one period; the sketch of the one-step TIPS method; SEM image and size distribution of PZT nanoparticles; X-ray diffraction of PZT nanoparticles and the cellular PP/PZT composite film with different PZT doping ratios; concrete current signals of 3D-CSA

DOI: 10.1021/acsami.8b14514
ACS Appl. Mater. Interfaces 2018, 10, 41070−41075

varied with days; uniformity of the sensor array based on the 3D-CSA; theory model derivation of the 3D-CSA; structural optimization of the cellular PP framework; performance optimization of the cellular PP/PZT composite framework; summary of the self-powered devices based on the piezoelectric effect and their pressure sensitivity (PDF)

Working principle of the 3D-CSA in one cycle (AVI)

3D-CSA for measuring the human heartbeat (AVI)

Self-powered 3D-CSA for eye blinking monitoring (AVI)

3D-CSA for tactile sensing (AVI)

AUTHOR INFORMATION

Corresponding Authors

*E-mail: weili1812@swjtu.edu.cn (W.D.).

*E-mail: chenjun@stanford.edu, junchenwelcome@gmail.com (J.C.).

*E-mail: wqyang@swjtu.edu.cn (W.Y.).

ORCID

Jun Chen: 0000-0002-3439-0495

Weiqing Yang: 0000-0001-8828-9862

Notes

The authors declare no competing financial interest.

ACKNOWLEDGMENTS

W.Y., J.C., and W.D. guided the reserach and supervised the whole project. This research was financially supported by the National Natural Science Foundation of China (no. 61801403), the Independent Research Project of State Key Laboratory of Traction Power (no. 2017TPL_Z04), and the Fundamental Research Funds for the Central Universities of China (nos. 2682017CY06, 2682017ZDPY01 and 2682017CX071). The authors gratefully acknowledge the Analysis and Testing Center of Southwest Jiaotong University.

REFERENCES

(1) Ko, H. C.; Stoykovich, M. P.; Song, J.; Malyarchuk, V.; Choi, W. M.; Yu, C.-J.; Geddes, J. B., 3rd; Xiao, J.; Wang, S.; Huang, Y.; Rogers, J. A. A Hemispherical Electronic Eye Camera Based on Compressible Silicon Optoelectronics. *Nature* **2008**, *454*, 748−753.

(2) Rogers, J. A.; Someya, T.; Huang, Y. Materials and Mechanics for Stretchable Electronics. *Science* **2010**, *327*, 1603−1607.

(3) Xu, S.; Zhang, Y.; Jia, L.; Mathewson, K. E.; Jang, K.-I.; Kim, J.; Fu, H.; Huang, X.; Chava, P.; Wang, R.; Bhole, S.; Wang, L.; Na, Y. J.; Guan, Y.; Flavin, M.; Han, Z.; Huang, Y.; Rogers, J. A. Soft Microfluidic Assemblies of Sensors, Circuits, and Radios for the Skin. *Science* **2014**, *344*, 70−74.

(4) Tee, B. C.-K.; Chortos, A.; Berndt, A.; Nguyen, A. K.; Tom, A.; McGuire, A.; Lin, Z. C.; Tien, K.; Bae, W.-G.; Wang, H.; Mei, P.; Chou, H.-H.; Cui, B.; Deisseroth, K.; Ng, T. N.; Bao, Z. A Skin-Inspired Organic Digital Mechanoreceptor. *Science* **2015**, *350*, 313−316.

(5) Chortos, A.; Liu, J.; Bao, Z. Pursuing Prosthetic Electronic Skin. *Nat. Mater.* **2016**, *15*, 937−950.

(6) Gao, W.; Emaminejad, S.; Nyein, H. Y. Y.; Challa, S.; Chen, K.; Peck, A.; Fahad, H. M.; Ota, H.; Shiraki, H.; Kiriya, D.; Lien, D.-H.; Brooks, G. A.; Davis, R. W.; Javey, A. Fully Integrated Wearable Sensor Arrays for Multiplexed in Situ Perspiration Analysis. *Nature* **2016**, *529*, 509−514.

(7) Jang, K.-I.; Li, K.; Chung, H. U.; Xu, S.; Jung, H. N.; Yang, Y.; Kwak, J. W.; Jung, H. H.; Song, J.; Yang, C.; Wang, A.; Liu, Z.; Lee, J. Y.; Kim, B. H.; Kim, J.-H.; Lee, J.; Yu, Y.; Kim, B. J.; Jang, H.; Yu, K. J.; Kim, J.; Lee, J. W.; Jeong, J.-W.; Song, Y. M.; Huang, Y.; Zhang, Y.; Rogers, J. A. Self-Assembled Three Dimensional Network Designs for Soft Electronics. *Nat. Commun.* **2017**, *8*, 15894.

(8) Lei, T.; Pochorovski, I.; Bao, Z. Separation of Semiconducting Carbon Nanotubes for Flexible and Stretchable Electronics Using Polymer Removable Method. *Acc. Chem. Res.* **2017**, *50*, 1096−1104.

(9) Rogers, J. A. Wearable Electronics: Nanomesh On-Skin Electronics. *Nat. Nanotechnol.* **2017**, *12*, 839−840.

(10) Xu, J.; Wang, S.; Wang, G.-J. N.; Zhu, C.; Luo, S.; Jin, L.; Gu, X.; Chen, S.; Feig, V. R.; To, J. W. F.; Rondeau-Gagné, S.; Park, J.; Schroeder, B. C.; Lu, C.; Oh, J. Y.; Wang, Y.; Kim, Y.-H.; Yan, H.; Sinclair, R.; Zhou, D.; Xue, G.; Murmann, B.; Linder, C.; Cai, W.; Tok, J. B.-H.; Chung, J. W.; Bao, Z. Highly Stretchable Polymer Semiconductor Films Through the Nanoconfinement Effect. *Science* **2017**, *355*, 59−64.

(11) Hu, H.; Zhu, X.; Wang, C.; Zhang, L.; Li, X.; Lee, S.; Huang, Z.; Chen, R.; Chen, Z.; Wang, C.; Gu, Y.; Chen, Y.; Lei, Y.; Zhang, T.; Kim, N. H.; Guo, Y.; Teng, Y.; Zhou, W.; Li, Y.; Nomoto, A.; Sternini, S.; Zhou, Q.; Pharr, M.; di Scalea, F. L.; Xu, S. Stretchable Ultrasonic Transducer Arrays for Three-Dimensional Imaging on Complex Surfaces. *Sci. Adv.* **2018**, *4*, No. eaar3979.

(12) Wang, C.; Wang, C.; Huang, Z.; Xu, S. Materials and Structures toward Soft Electronics. *Adv. Mater.* **2018**, *30*, 1801368 DOI: 10.1002/adma.201801368.

(13) Wang, S.; Xu, J.; Wang, W.; Wang, G.-J. N.; Rastak, R.; Molina-Lopez, F.; Chung, J. W.; Niu, S.; Feig, V. R.; Lopez, J.; Lei, T.; Kwon, S.-K.; Kim, Y.; Foudeh, A. M.; Ehrlich, A.; Gasperini, A.; Yun, Y.; Murmann, B.; Tok, J. B.-H.; Bao, Z. Skin Electronics from Scalable Fabrication of An Intrinsically Stretchable Transistor Array. *Nature* **2018**, *555*, 83−88.

(14) Yang, Y.; Gao, W. Wearable and Flexible Electronics for Continuous Molecular Monitoring. *Chem. Soc. Rev.* **2018**, DOI: 10.1039/c7cs00730b.

(15) Ha, M.; Lim, S.; Ko, H. Wearable and Flexible Sensors for User-Interactive Health-Monitoring Devices. *J. Mater. Chem. B* **2018**, *6*, 4043−4064.

(16) Lee, Y.; Park, J.; Cho, S.; Shin, Y.-E.; Lee, H.; Kim, J.; Myoung, J.; Cho, S.; Kang, S.; Baig, C.; Ko, H. Flexible Ferroelectric Sensors with Ultrahigh Pressure Sensitivity and Linear Response over Exceptionally Broad Pressure Range. *ACS Nano* **2018**, *12*, 4045−4054.

(17) Wang, J.; Li, S.; Yi, F.; Zi, Y.; Lin, J.; Wang, X.; Xu, Y.; Wang, Z. L. Sustainably Powering Wearable Electronics Solely by Biomechanical Energy. *Nat. Commun.* **2016**, *7*, 12744.

(18) Fan, F. R.; Tang, W.; Wang, Z. L. Flexible Nanogenerators for Energy Harvesting and Self-Powered Electronics. *Adv. Mater.* **2016**, *28*, 4283−4305.

(19) Ha, M.; Lim, S.; Cho, S.; Lee, Y.; Na, S.; Baig, C.; Ko, H. Skin-Inspired Hierarchical Polymer Architectures with Gradient Stiffness for Spacer-Free, Ultrathin, and Highly Sensitive Triboelectric Sensors. *ACS Nano* **2018**, *12*, 3964−3974.

(20) Xu, S.; Zhang, Y.; Cho, J.; Lee, J.; Huang, X.; Jia, L.; Fan, J. A.; Su, Y.; Su, J.; Zhang, H.; Cheng, H.; Lu, B.; Yu, C.; Chuang, C.; Kim, T.-i.; Song, T.; Shigeta, K.; Kang, S.; Dagdeviren, C.; Petrov, I.; Braun, P. V.; Huang, Y.; Paik, U.; Rogers, J. A. Stretchable Batteries with Self-similar Serpentine Interconnects and Integrated Wireless Recharging Systems. *Nat. Commun.* **2013**, *4*, 1543.

(21) Li, H.; Ding, Y.; Ha, H.; Shi, Y.; Peng, L.; Zhang, X.; Ellison, C. J.; Yu, G. An All-Stretchable-Component Sodium-Ion Full Battery. *Adv. Mater.* **2017**, *29*, 1700898.

(22) Liu, W.; Chen, J.; Chen, Z.; Liu, K.; Zhou, G.; Sun, Y.; Song, M.-S.; Bao, Z.; Cui, Y. Stretchable Lithium-Ion Batteries Enabled by Device-Scaled Wavy Structure and Elastic-Sticky Separator. *Adv. Energy Mater.* **2017**, *7*, 1701076.

(23) Wang, X.; Lu, X.; Liu, B.; Chen, D.; Tong, Y.; Shen, G. Flexible Energy-Storage Devices: Design Consideration and Recent Progress. *Adv. Mater.* **2014**, *26*, 4763−4782.

(24) Wu, H.; Zhuo, D.; Kong, D.; Cui, Y. Improving Battery Safety by Early Detection of Internal Shorting with A Bifunctional Separator. *Nat. Commun.* **2014**, *5*, 5193.

(25) Kong, D.; Li, X.; Zhang, Y.; Hai, X.; Wang, B.; Qiu, X.; Song, Q.; Yang, Q.-H.; Zhi, L. Encapsulating V_2O_5 into Carbon Nanotubes Enables the Synthesis of Flexible High-Performance Lithium Ion Batteries. *Energy Environ. Sci.* **2016**, *9*, 906−911.
(26) Liu, Z.; Li, H.; Zhu, M.; Huang, Y.; Tang, Z.; Pei, Z.; Wang, Z.; Shi, Z.; Liu, J.; Huang, Y.; Zhi, C. Towards Wearable Electronic Devices: A Quasi-Solid-State Aqueous Lithium-Ion Battery with Outstanding Stability, Flexibility, Safety and Breathability. *Nano Energy* **2018**, *44*, 164−173.
(27) Wang, Z. L.; Song, J. Piezoelectric Nanogenerators Based on Zinc Oxide Nanowire Arrays. *Science* **2006**, *312*, 242−246.
(28) Yang, R.; Qin, Y.; Li, C.; Zhu, G.; Wang, Z. L. Converting Biomechanical Energy into Electricity by A Muscle-Movement-Driven Nanogenerator. *Nano Lett.* **2009**, *9*, 1201−1205.
(29) Pu, X.; Liu, M.; Chen, X.; Sun, J.; Du, C.; Zhang, Y.; Zhai, J.; Hu, W.; Wang, Z. L. Ultrastretchable, Transparent Triboelectric Nanogenerator as Electronic Skin for Biomechanical Energy Harvesting and Tactile Sensing. *Sci. Adv.* **2017**, *3*, No. e1700015.
(30) Chen, J.; Huang, Y.; Zhang, N.; Zou, H.; Liu, R.; Tao, C.; Fan, X.; Wang, Z. L. Micro-cable Structured Textile for Simultaneously Harvesting Solar and Mechanical Energy. *Nat. Energy* **2016**, *1*, 16138.
(31) Fan, F.-R.; Tian, Z.-Q.; Lin Wang, Z. Flexible Triboelectric Generator. *Nano Energy* **2012**, *1*, 328−334.
(32) Wu, W.; Wang, L.; Li, Y.; Zhang, F.; Lin, L.; Niu, S.; Chenet, D.; Zhang, X.; Hao, Y.; Heinz, T. F.; Hone, J.; Wang, Z. L. Piezoelectricity of single-atomic-layer MoS2 for energy conversion and piezotronics. *Nature* **2014**, *514*, 470−474.
(33) Chen, J.; Zhu, G.; Yang, J.; Jing, Q.; Bai, P.; Yang, W.; Qi, X.; Su, Y.; Wang, Z. L. Personalized Keystroke Dynamics for Self-Powered Human-Machine Interfacing. *ACS Nano* **2015**, *9*, 105−116.
(34) Wu, W.; Wen, X.; Wang, Z. L. Taxel-Addressable Matrix of Vertical-Nanowire Piezotronic Transistors for Active and Adaptive Tactile Imaging. *Science* **2013**, *340*, 952−957.
(35) Chen, J.; Wang, Z. L. Reviving Vibration Energy Harvesting and Self-Powered Sensing by a Triboelectric Nanogenerator. *Joule* **2017**, *1*, 480−521.
(36) Yang, J.; Chen, J.; Su, Y.; Jing, Q.; Li, Z.; Yi, F.; Wen, X.; Wang, Z.; Wang, Z. L. Eardrum-Inspired Active Sensors for Self-Powered Cardiovascular System Characterization and Throat-Attached Anti-Interference Voice Recognition. *Adv. Mater.* **2015**, *27*, 1316−1326.
(37) Ren, Z.; Nie, J.; Shao, J.; Lai, Q.; Wang, L.; Chen, J.; Chen, X.; Wang, Z. L. Fully Elastic and Metal-Free Tactile Sensors for Detecting both Normal and Tangential Forces Based on Triboelectric Nanogenerators. *Adv. Funct. Mater.* **2018**, *28*, 1802989.
(38) Nie, J.; Ren, Z.; Shao, J.; Deng, C.; Xu, L.; Chen, X.; Li, M.; Wang, Z. L. Self-Powered Microfluidic Transport System Based on Triboelectric Nanogenerator and Electrowetting Technique. *ACS Nano* **2018**, *12*, 1491−1499.
(39) Chen, X.; Liu, L.; Feng, Y.; Wang, L.; Bian, Z.; Li, H.; Wang, Z. L. Fluid eddy Induced Piezo-Promoted Photodegradation of Organic Dye Pollutants in Wastewater on ZnO Nanorod Arrays/3D Ni Foam. *Mater. Today* **2017**, *20*, 501−506.
(40) Chen, X.; Jiang, T.; Yao, Y.; Xu, L.; Zhao, Z.; Wang, Z. L. Stimulating Acrylic Elastomers by a Triboelectric Nanogenerator - Toward Self-Powered Electronic Skin and Artificial Muscle. *Adv. Funct. Mater.* **2016**, *26*, 4906−4913.
(41) Ma, X.; Zhang, X.; Fang, P. Flexible Film-Transducers Based on Polypropylene Piezoelectrets: Fabrication, Properties, and Applications in Wearable Devices. *Sens. Actuator A-Phys.* **2017**, *256*, 35−42.
(42) Li, W.; Zhao, S.; Wu, N.; Zhong, J.; Wang, B.; Lin, S.; Chen, S.; Yuan, F.; Jiang, H.; Xiao, Y.; Hu, B.; Zhou, J. Sensitivity-Enhanced Wearable Active Voiceprint Sensor Based on Cellular Polypropylene Piezoelectret. *ACS Appl. Mater. Interfaces* **2017**, *9*, 23716−23722.
(43) Li, W.; Torres, D.; Wang, T.; Wang, C.; Sepúlveda, N. Flexible and Biocompatible Polypropylene Ferroelectret Nanogenerator (FENG): On the Path Toward Wearable Devices Powered by Human Motion. *Nano Energy* **2016**, *30*, 649−657.
(44) Zhong, Q.; Zhong, J.; Cheng, X.; Yao, X.; Wang, B.; Li, W.; Wu, N.; Liu, K.; Hu, B.; Zhou, J. Paper-Based Active Tactile Sensor Array. *Adv. Mater.* **2015**, *27*, 7130−7136.
(45) Liu, Y.; He, K.; Chen, G.; Leow, W. R.; Chen, X. Nature-Inspired Structural Materials for Flexible Electronic Devices. *Chem. Rev.* **2017**, *117*, 12893−12941.
(46) Someya, T.; Bao, Z.; Malliaras, G. G. The Rise of Plastic Bioelectronics. *Nature* **2016**, *540*, 379−385.

DOI: 10.1021/acsami.8b14514
ACS Appl. Mater. Interfaces 2018, 10, 41070−41075